journal

J. Am. Ceram. Soc., 1–7 (2012)
DOI: 10.1111/jace.12021

Tuning Hydrophobicity with Honeycomb Surface Structure and Hydrophilicity with CF_4 Plasma Etching for Aerosol-Deposited Titania Films

Do-Yeon Kim,[‡] Jung-Jae Park,[‡] Jong-Gun Lee,[‡] Min-Wook Lee,[‡] Ho-Young Kim,[‡] Joon-Ho Oh,[§] Tae-Yeon Seong,[§] Donghwan Kim,[§] Scott C. James,[¶] Maikel F. A. M.van Hest,[‖] Sanjeev Chandra,[‡‡] and Sam S. Yoon[‡,†]

[‡]School of Mechanical Engineering, Korea University, Seoul 136-713, Korea

[§]School of Materials Science and Engineering, Korea University, Seoul 136-713, Korea

[¶]Thermal Fluid Science & Engineering, Sandia National Laboratories, Livermore, California 94551-0969

[‖]National Renewable Energy Laboratory, Golden, Colorado 80401

[‡‡]Department of Mechanical & Industrial Engineering, University of Toronto, 5 King's College Rd., Toronto, ON M5S 3G8, Canada

A tunable surface that promotes either hydrophobic or hydrophilic behavior of TiO_2 films is produced with aerosol deposition. This process is capable of mass production by high-speed coating at room temperature without any wet chemicals, and therefore the process has the potential to be economically viable, energy efficient, and environmentally friendly. Functional TiO_2 films between 1 and 18 μm thick are produced by directly depositing dry, 1-μm TiO_2 powders accelerated through a supersonic nozzle. Tunable film morphology due to a rough honeycomb surface structure yields variable water contact angles. When plasma treated with CF_4, the films exhibit superhydrophilicity despite the rough honeycomb surface structure. Superhydrophilicity is due to the incorporation of fluorine in the film as shown using XPS.

I. Introduction

Photocatalysis of titanium dioxide (TiO_2) has many industrial applications because of its high photoactivity, stability, and low cost. When exposed to ultraviolet light, TiO_2 exhibits a distinct photochemical behavior known as photo-induced hydrophilicity. Photogenerated holes can react with (absorb) water to produce OH^- radicals. This reaction also produces Ti^{3+} and oxygen vacancies, which in turn adsorb water molecules at defect sites, and further promote hydrophilicity. This photo-induced hydrophilicity has many practical applications found in self-cleaning, deodorizing, self-sterilizing, air-cleaning, and anti-fogging products.[1] TiO_2 coatings also have potential uses in water-splitting electrodes and dye-sensitized solar cells.[2]

Conventional methods of TiO_2 powder deposition can be either non-vacuum or vacuum-based. Non-vacuum methods include doctor blading,[3] dip coating,[4] spin coating,[5] screen printing,[6] and sol–gel[7] approaches whereas vacuum-based methods include chemical vapor deposition,[8] pulsed laser deposition,[9] and sputtering[10]. All of these methods require a high-temperature post-annealing process (sintering) to enhance film recrystallization. All of these methods have shortcomings. First, energy requirements for these processes are significant. Second, flexible polymer substrates cannot be readily used because of the high temperature requirements; this prohibits use of roll-to-roll flexible substrates, which are needed for low-cost mass production of functional materials. A low-temperature coating process that does not require post processing would facilitate energy-efficient, environmentally friendly, and low-cost production.

Aerosol deposition (AD) avoids these shortcomings by promoting adhesion and cohesion between TiO_2 powders and substrates[11,12] through simple impact of powder particles onto a substrate; no high-temperature process is necessary. AD uses a high-velocity gas jet to accelerate feedstock powder to a sufficiently high velocity such that high-density coatings (or porous coating upon inclusion of organic binders or surfactants) are formed at low temperatures. AD is a relatively low-cost process that yields dense nanocrystalline films under the proper conditions. AD has typically been used on smaller devices like micro-actuators, embedded passive components for high-frequency devices, and high-speed optical modulators even though it can be applied to large-scale substrates such as automobile components and building materials.

Fan *et al.*[2,13,14] investigated characteristics and microstructural features of AD TiO_2 films for dye-sensitized solar-cell applications. They demonstrated increased efficiency after a post-annealing treatment for porosity control through addition of polyethylene glycol. They also noted that TiO_2 film thickness had a profound effect on the cell efficiency, which was consistent with the results obtained by Nazeeruddin *et al.*[3] Ryu *et al.*[15] demonstrated that contact angle of water droplets on an AD TiO_2 film decreased with UV-light exposure time. Hashimoto *et al.*[1] showed that hydrophilicity is an interfacial phenomenon, not a bulk property. However, to our knowledge, altering wettability of AD TiO_2 film by varying the honeycomb structure and surface modification has not been studied. This "tunable" wettability can be of great benefit to self-cleaning applications.

This study, for the first time investigates the effects of the honeycomb structure and surface modification by CF_4 plasma etching on film wettability. The optimized supersonic nozzle, based on a computational fluid dynamics solution, was used to deposit TiO_2 particles onto a substrate. The optimized nozzle yields the fastest, stable, most uniform gas flow.[16] Surface morphologies (roughness) and cross-sectional views of various-thickness films are visualized using a scanning electron microscope (SEM). Hydrophilic/hydrophobic

P. Gouma—contributing editor

Manuscript No. 31588. Received June 15, 2012; approved September 6, 2012.
[†]Author to whom correspondence should be addressed. e-mail: skyoon@korea.ac.kr

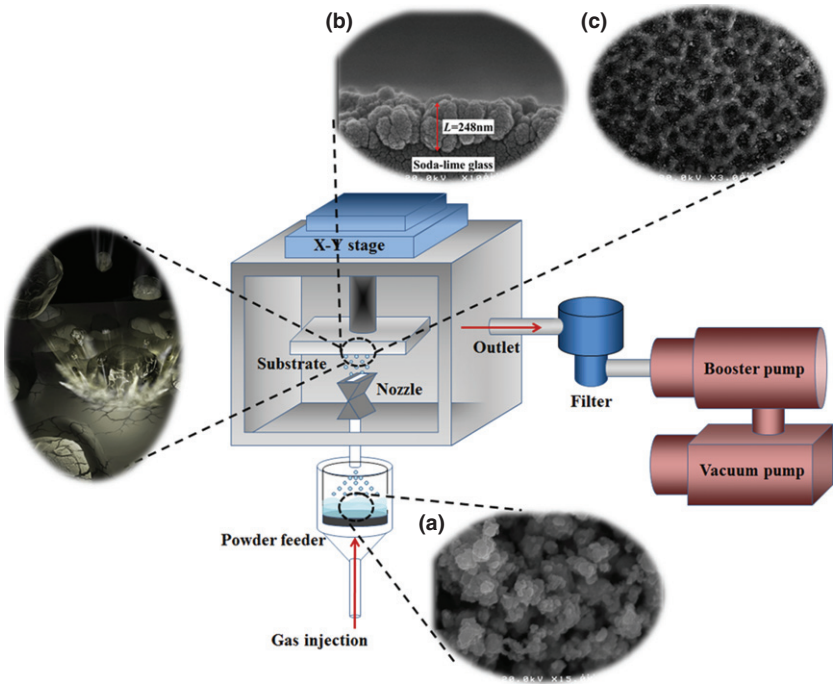

Fig. 1. Schematic of the AD system (a) SEM of the TiO_2 powder (b) side and (c) top views of an AD TiO_2 film showing the 3D cross-linked honeycomb structure.

control of the film is described. We also demonstrate that a superhydrophilic surface can be fabricated by surface modification with CF_4 plasma etching.

II. Experimental Setup

Figure 1 is a schematic of the AD experimental setup, comprising gas tank, fluidized-bed powder feeder, nozzle, vacuum chamber, 2D *x-y* stage, booster pump, and vacuum pump. TiO_2 powder is premixed with dehumidified air in a fluidized bed and fed into the nozzle with an injection absolute pressure of $P_o = 2$ bar. Replacing the dry-air with a lighter inert gas, like helium, could increase gas speed and the corresponding TiO_2 particle velocity if needed. The average particle impact velocity is around 200 m/s.[17,18] TiO_2 particles are accelerated through the supersonic nozzle and the particle-laden air is injected into the deposition chamber evacuated by vacuum and booster pumps. The deposition chamber was evacuated to minimize air drag; it was maintained in the range of $0.35 \leq P_{amb} \leq 15$ Torr. This low chamber pressure can only be maintained up to an injection flow rate of about 20 L/min. Deposition conditions are summarized in Table I. Schlieren images at the nozzle exit confirmed the supersonic speed of the particles because of the presence of shocks (data not shown here).[16,19] The nozzle dimensions are listed in Table II. Figure 1(a) shows an SEM of a commercially available TiO_2 powder; a mixture of 60% anatase and 40% rutile. Agglomeration is observed; however, to break up particle clusters, the powder was mixed with water in a rotary evaporator, calcinated at 400°C, then ball-milled for 24 h. This resulted in an average particle size of ~1 μm, according to the particle size analyzer system (LA-950-V2; Horiba, Hakata-ku Fukuoka, Japan). Such pretreated powders are expected to improve the deposition rate.[11] The SEM image shows an average particle size of 0.1 μm prior to agglomeration, which is much smaller than the size measured by the particle size analyzer, which measures the agglomerates.

Mass flow rates of the supply air ranged from 1 to 20 L/min, which also specifies the power feeding rate; they are linearly proportional. For the average particle size of $d_{50} = 1$ μm, $Stk < 0.2$, which implies that the particles attain in excess of 90% of the gas flow speed.[19] The Stokes number, $Stk = \tau_p/\tau_g$, is the ratio of particle response time to the surrounding flow, $\tau_p = \rho_p D^2/(18\ \mu_g)$, to the characteristic time of the surrounding flow, $\tau_g = d/u_{g,exit}$ (ρ_p and D are the particle density and diameter, respectively; μ_g is the gas dynamic viscosity, and d and $u_{g,exit}$ are the nozzle exit diameter and gas speed). The substrate is situated 5 mm away from the nozzle, which was installed onto a maneuvering stage that required ~50 s to travel 5 cm (i.e., the nozzle passing/scanning speed is about 1 mm/s). The moving substrate traversed the path of the fixed nozzle up to $N = 14$ times to form multiple AD layers for a total thickness of almost 13.5 μm (~1 μm per pass). Although a uniform distribution of powder is desired across the nozzle exit, it is likely that particle number density at the nozzle center is greater than that at the periphery. All TiO_2 films were manufactured at room temperature on soda-lime glass substrates with surface area and roughness of 2.5 cm × 7.5 cm and Ra < 0.1 nm, respectively. Substrates were cleaned in an ultrasonic acetone bath for 10 minutes before use.

Table I. Typical Deposition Conditions

Pressure in deposition chamber [Torr]	0.35–15
Propellant gas	Air
Powder	TiO_2
Stand-off distance (mm)	5
Gas temperature (°C)	20
Consumption of propellant gas [l/min]	1–20
Traverse speed (mm/s)	1.0
Number of passes	4–14
Deposition area (mm^2)	20 × 20

Table II. Nozzle Dimension Details

Nozzle dimension	Nozzle
Throat area (mm^2)	1 × 20
Exit area (mm^2)	5 × 20
Diverging length (mm)	70

A radio frequency of 13.56 MHz was applied to the bottom electrode, which was maintained at 20°C. TiO_2 films (each sample was 2.5 cm × 2.5 cm) were placed inside the operating chamber and were plasma-etched with CF_4 reactive gas (50 sccm, 100 W, 15 mTorr) for etching times ranging from t_{etch} = 1 to 10 min in intervals of Δt_{etch} = 1 min. The plasma-etching system maintained vacuum conditions (5.0×10^{-5} Torr) with both a rotary and turbo-molecular pump.

The microstructures and crystallinity of the deposited TiO_2 films were characterized using both a high-resolution SEM (HRSEM, XL30SFEG; Phillips Co., Amsterdam, Holland at 10 kV) and X-ray diffraction (XRD; D/MAX-2500, Rigaku, Tokyo, Japan), using Cu KR-α line with an angular domain between 20° and 50° (2θ). An atomic force microscope (AFM; XE-100, Park Systems, Suwon, South Korea) was used to measure the surface roughness of the substrate. An optical microscope was used to measure the water contact angle after UV light (λ = 365 nm) exposure.

III. Results and Discussion

Upon high-speed impact of particles onto the substrate, they disintegrate into nano-sized sub-grains whose sizes can be approximated through recrystallization theory.[20] Because of the high impact speeds, pressures at the impact point up to a few GPa can be achieved.[21] Dislocated sub-grains quickly adhere to the substrate before re-solidification. Fan *et al.*[2] speculated that the impact of a series of sprayed particles is the primary mechanism for densification of the film. Because particle velocities are always less than the gas velocity, the gas velocity must be well over the "critical velocity" to achieve high-quality coating (successful bonding of a solid particle onto the substrate). A typical range of critical impact velocities for ceramic materials is between 150 and 500 m/s.[11] The primary objective of this study was to investigate functionality of the AD film; hydrophobicity and hydrophilicity (by water-droplet contact angle proxy). The honeycomb structure and its roughness are controlled by the number of passes, N, of the nozzle over the substrate.

Figure 2 shows the cross-sectional morphologies of nanocrystalline TiO_2 films deposited onto a soda-lime glass substrate. TiO_2 particles are assumed to fracture and flatten upon impact yielding a fairly dense structure with few voids, but surface morphology is highly undulating due to a honeycomb structure. Voids may exist due to insufficient compaction and lack of coalescence between TiO_2 particles; films are not perfectly hermetic.

All coatings showed sufficient adhesion and were not detached during a standard direct pull-off test; the average value of the maximum hardness was 7.23 GPa and the Young's modulus was about 250 GPa measured using a Nanoindenter G200 (Agilent Technologies, Santa Clara, CA; Berkovich diamond indenter tip). The maximum indentation depth was 1000 nm, and the surface approach velocity was 5 nm/s.

The number of spray passes (i.e., N = 4, 10, or 14 layers) and the air flowrate (Q = 10, 15, or 20 L/min) were varied to observe their effects on the film thicknesses. Although the trend of increasing film thickness with N is apparent in Fig. 3, the thickness per layer does not monotonically increase with Q. This is due to two competing processes. First, higher flow rates eject more TiO_2 particles that build the film more quickly. However, there is an equipment limitation; the vacuum and booster pumps cannot maintain the low pressure in the system required for AD under high nozzle flow rates. Films formed for Q = 20 L/min is actually thinner than when Q = 15 L/min (given equal N). An experiment run at Q = 30 L/min did not form a film at all because of the elevated pressure inside the chamber, which significantly slowed the particle impact velocity with an increased air drag. For our system, there is an optimal flow rate around Q = 15 L/min.

Figure 4(a) shows a typical honeycomb surface structure of AD TiO_2. This three-dimensional honeycomb structure was universally observed and repeatedly fabricated for all AD TiO_2 films as long as the film thickness was in excess of 3 μm or $N \geq 4$. This honeycomb structure is *self-assembled* and not intentionally designed as it is for nanotube fabrication[22–26] [see Figs. 4(d) and (e)]. This type of highly cross-linked *undulating* structure can be of a great use for applications in catalysis, separation engineering, chemical reactors, chemical sensing, and electrochemical cells.[27–30] Specifically, because of the relatively large surface area of this honeycomb structure, the film may exhibit exceptionally superior physical and chemical properties such as enhanced ion transport rates and increased interfacial resistance for electrochemical cells.[31,32] The mechanism behind this structural development is not completely understood. One hypothesis is based on the fact that AD TiO_2 has a high affinity for itself. During film development, TiO_2 particles are more likely to adhere to previously deposited TiO_2 to yield the honeycomb-like morphology. It is possible that this honeycomb structure can increase the photocatalytic effect by increasing film surface area under UV illumination. However, without UV, increased roughness in fact increases contact angle, thereby promoting hydrophobicity; this yields a tunable feature of our TiO_2 film.

Figure 5 shows the XRD patterns of the raw TiO_2 powder (bottom curve), which is 60% anatase and 40% rutile, and the AD film (top curve). The raw powder exhibits strong anatase A (101) and rutile R (110) structures; crystallite sizes are listed in Table III. Although the AD film reveals the same anatase and rutile, a new brookite structure has appeared indicating that there has been some local heating due to particle impact. Even though there was no post

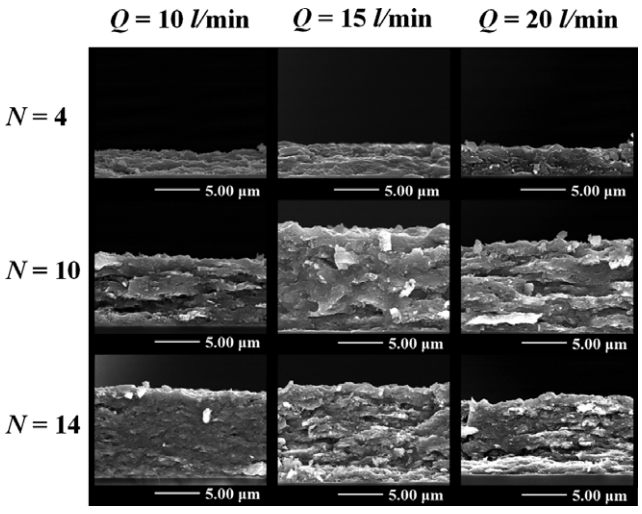

Fig. 2. SEM cross-sectional micrographs of TiO_2 films on a soda-lime glass substrate.

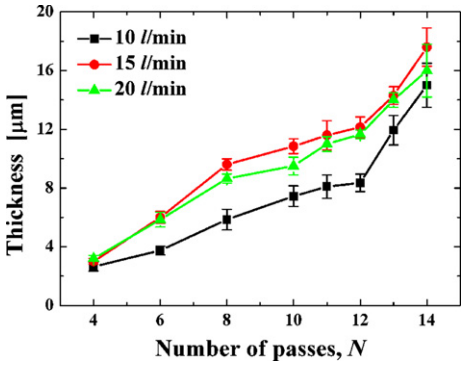

Fig. 3. TiO_2 film thickness variation with N for various flow rates.

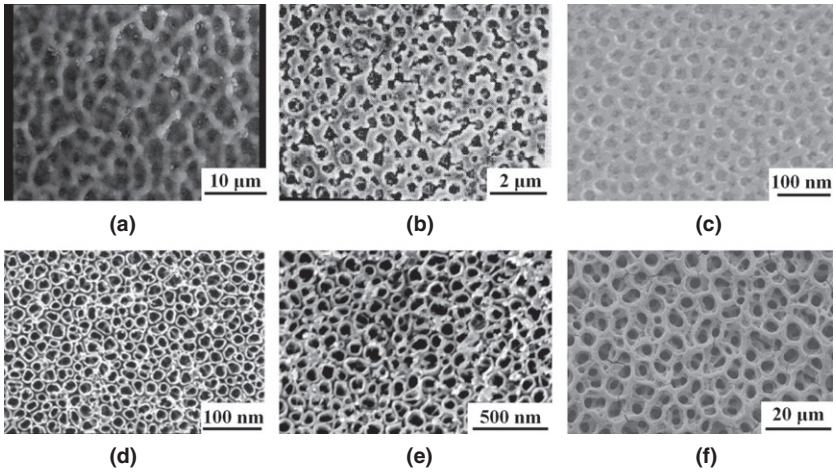

Fig. 4. SEM surface micrographs of TiO_2 films of the honeycomb structure designed by various methods. (a) Aerosol deposition TiO_2 film. (b) TiO_2 films on soda-lime glass prepared by the sol-gel method from alkoxide solutions containing polyethylene glycol (PEG).[22] (c) SiO_2/TiO_2 bilayers prepared by the sol-gel method. The SiO_2 layer is methyl-functionalized nanoporous. The TiO_2 layer is nanoperforated.[23] (d) TiO_2 nanotube arrays prepared by a potentiostatic anodization in a two-electrode electrochemical cell.[26] (e) TiO_2 nanotube arrays made by anodic oxidation of titanium in fluoride-based electrolytes.[24] (f) The manganese-oxide films electro-spray-deposited using precursor solutions of 0.01 M $Mn(CH_3COO)_2$ dissolved in propylene at the substrate temperature of 170° C.[25]

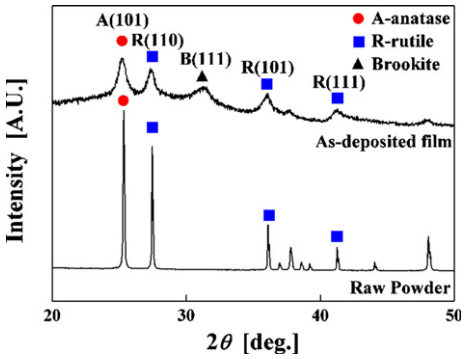

Fig. 5. XRD patterns of the raw powder and a TiO_2 film on the soda-lime substrate.

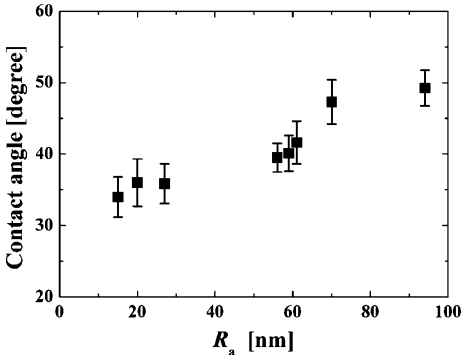

Fig. 6. Effect of R_a on contact angle when Q = 20 L/min without UV light.

Table III. Size of the Crystalline TiO_2 Lattice

	Crystal size (nm)	
TiO_2 lattice	Powder	As-deposited film
Anatase (101)	68.9	13.8
Rutile (110)	83.1	15.7

annealing of our aerosol-deposited titania films, local heating due to particle impact can yield brookite (CAS card no. 29-1360) and srilankite (CAS card no. 21-1236) phases.[33] The brookite phase has superior electrochemical properties (such as photo-induced hydrophilicity) originating from the nature of its surface states.[34–36] The induced brookite phase is another advantage of the AD process.

The peaks for the AD film are broader and less intense than those for the raw powder, which has narrow, intense peaks. In general, a narrow, intense peak indicates relatively large, well-crystallized grains. Table III indicates that the crystallite size has substantially decreased after particle impact. The Debye-Scherrer relation states that broad XRD peaks imply that nano-sized grains formed after disintegration of the impacting particles,[37] consistent with what is expected from AD. The AD coating process disintegrates the original TiO_2 powder resulting in a notable reduction in grain size. High residual stresses in nano-sized grains could potentially shift the XRD peaks, but no major shifts were observed.

Figure 6 reinforces that contact angle increases slightly with surface roughness (no UV illumination). In general, hydrophobicity can be controlled by tuning surface energy and/or surface roughness.[38] For example, a substrate of low surface energy aided by a roughened surface can yield a superhydrophobic state (e.g., the regularly aligned close hexagonally packed CF_3 groups has a surface energy of 6.7 mJ/m and a contact angle >150°). Air trapped among the roughened surfaces hinders direct contact of liquid and solid. For example, the film can be purposely rough-coated to promote hydrophobicity. However, with UV illumination, increased roughness can, instead, promote hydrophilicity through increased photo-induced areas as long as $R_a < 100$ nm.[1] To ascertain the dominance of either roughness-driven hydrophobicity or UV-driven hydrophilicity, we measured the water contact angle as a function of roughness for various UV light exposure times. The contact angle increased (i.e., become more hydrophobic) with increasing roughness for all UV exposure times suggesting that the honeycomb surface roughness takes precedence over UV-driven hydrophilicity.

As noted earlier, two distinctive features of TiO_2 are its photocatalytic response and hydrophilicity. Watanabe *et al.*[39] suggested that the photocatalytic behavior is more of a bulk property whereas hydrophilicity is essentially an interfacial property. Photocatalytic TiO_2 decomposes volatile organic compounds[40] whereas hydrophilicity is a phenomenon whereby water drops spread easily and have a low contact angle. Both the photocatalytic behavior and hydrophilicity are activated when a TiO_2 film is exposed to UV light. However, even with-

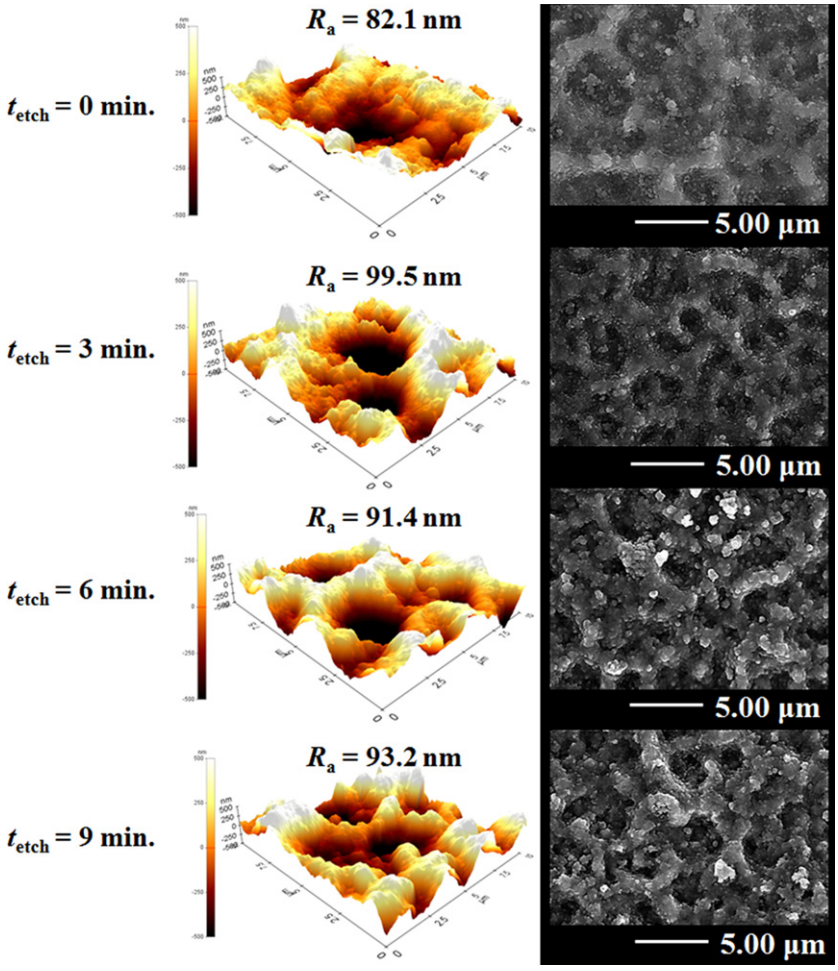

Fig. 7. AFM and SEM images for various etching times.

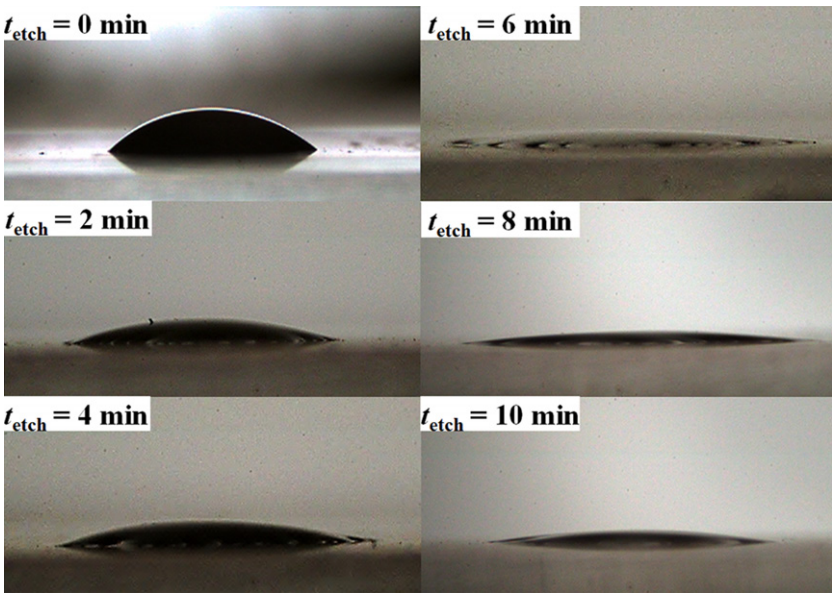

Fig. 8. Optical images of water contact angle for various CF_4 plasma etching times without UV light.

out the UV illumination, we show that TiO_2 films can retain high wettability if film surfaces are treated with CF_4 plasma etching, which seems counter to conventional thought because rougher surfaces are typically more hydrophilic.

In general, CF_4 plasma etching removes material from a surface yielding mesoscale roughness. Zhang *et al.*[41] used CF_4 plasma etching to roughen smooth TiO_2 films produced by a sol-gel method. They fabricated a hydrophobic, nanocolumnar morphology with octadecylphosphonic acid (ODP) treatment. Such a treated surface yielded a superhydrophobic surface without UV light exposure. Upon UV exposure, the superhydrophobic surface became superhydrophilic due to photocatalytic decomposition of the ODP monolayer. Our AD films are different from their TiO_2 films because of the

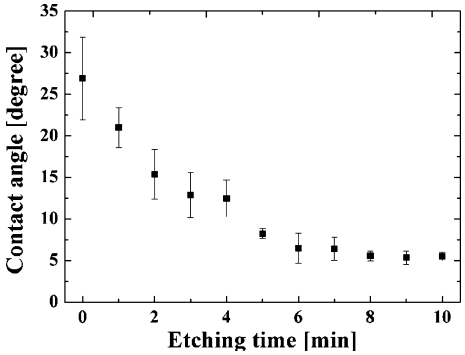

Fig. 9. Water contact angle for TiO_2 films etched using an CF_4 plasma without UV light.

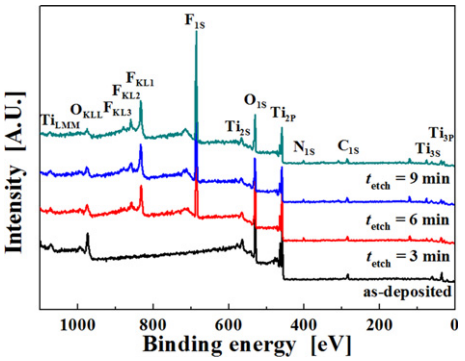

Fig. 10. XPS results for various etching times.

rough honeycomb structure. Our AD films are already hydrophobic and need no plasma etching to yield hydrophobicity. On the contrary, we used CF_4 plasma etching to create a hydrophilic surface. Unlike Zhang *et al.*,[41] our AFM and SEM images in Fig. 7 qualitatively show that there is no distinguishable effect of etching time ($1 \text{ min} \leq t_{etch} \leq 10 \text{ min}$) on film roughness and morphology (at least not in the microscopic sense).

Despite little change in surface morphology with respect to etching time, Figs. 8 and 9 show that etching time has a profound effect on wettability (increased hydrophilicity). Because this trend is opposite to the trend observed by Zhang *et al.*,[41] some other changes to the film must have occurred. While the Zhang *et al.*[41] films' roughnesses changed significantly, our films are no more or less rough after CF_4 plasma etching. XPS analysis of the films shown in Fig. 10 shows that significant amounts of fluorine are measurable in the plasma-exposed films. Films not exposed to the plasma do not show any fluorine. The presence of fluorine, limited to the surface of the film, enhances hydrophilicity because of fluorine's electro negativity. XPS data show that fluorine content increases with increased CF_4 etching time. This is consistent with the decreased contact angle with increased CF_4 plasma exposure time. Zhang *et al.*[41] did not observe this effect because their contact-angle change was dictated by a change in film roughness despite the change in surface fluorine concentration. This suggests that roughness is the controlling parameter in their case. In our AD films, which are already rough due to the honeycomb structure and no more or less rough upon etching, the effect of incorporating fluorine on the surface is clearly manifest as a decreased (hydrophilic) contact angle.

IV. Conclusions

Aerosol deposition has been used to deposit films from TiO_2 micropowders. No wet chemicals need be used, which facilitates films free of organics. The deposited films have rough, undulating surfaces and show a honeycomb-like structure. The roughness, and with that the water contact angle is dependent on the number of layers deposited. Films up to 18 μm thickness were deposited this way. The rough film is initially hydrophobic (water contact angles >35°), but can be made superhydrophilic by CF_4 plasma etching, which enriches the film surface with electronegative fluorine.

Acknowledgments

This work was supported by the Human Resources Development of the Korea Institute of Energy Technology Evaluation and Planning (KETEP, no. 20104010100640), National Research Foundation of Korea (NRF-2012-0001169), and the Converging Research Center Program through the Ministry of Education, Science and Technology (2010K000969). This work was also supported by NRF-2011-013-D00017 and 2010-0010217 grant funded by the Korean government (MEST) and by a grant from the cooperative R&D Program (B551179-08-03-00) funded by the Korea Research Council Industrial Science and Technology.

References

[1]K. Hashimoto, H. Irie, and A. Fujishima, "TiO_2 Photocatalysis: A Historical Overview and Future Prospects," *Jpn. J. Appl. Phys., Part 1*, **44** [12] 8269–85 (2005).

[2]S. Fan, G. Yang, C. Li, G. Liu, C. Li, and L. Zhang, "Characterization of Microstructure of Nano-TiO_2 Coating Deposited by Vacuum Cold Spraying," *J. Therm. Spray Technol.*, **15** [4] 513–7 (2006).

[3]M. K. Nazeeruddin, A. Kay, I. Rodicio, R. Humphry-Baker, E. Müller, P. Liska, N. Vlachopoulos, and M. Grätzel, "Conversion of Light to Electricity by cis-X2bis (2, 2′-bipyridyl-4, 4′-dicarboxylate) Ruthenium (II) Charge-Transfer Sensitizers (X= Cl-, Br-, I-, CN-, and SCN-) on Nanocrystalline Titanium Dioxide Electrodes," *J. Am. Ceram. Soc.*, **115** [14] 6382–90 (1993).

[4]P. Sawunyama, L. Jiang, A. Fujishima, and K. Hashimoto, "Photodecomposition of a Langmuir-Blodgett Film of Stearic Acid on TiO_2 Film Observed by In Situ Atomic Force Microscopy and FT-IR," *J. Phys. Chem. B*, **101** [51] 11000–3 (1997).

[5]T. Tatsuma, W. Kubo, and A. Fujishima, "Patterning of Solid Surfaces by Photocatalytic Lithography Based on the Remote Oxidation Effect of TiO_2," *Langmuir*, **18** [25] 9632–4 (2002).

[6]L. F. Cheng, Y. Wang, S. Y. Dai, Q. C. Wu, and K. J. Wang, "Preparation and Virtues of Nanocrystalline TiO_2 Porous Film and its Application in Solar Cell," *Chin. J. Mater. Res.*, **10**, 404–8 (1996).

[7]Z. Wang, U. Helmersson, and P.-O. Käll, "Optical Properties of Anatase TiO_2 Thin Films Prepared by Aqueous Sol-Gel Process at Low Temperature," *Thin Solid Films*, **405** [1–2] 50–4 (2002).

[8]S. Campbell, H. S. Kim, D. Gilmer, B. He, T. Ma, and W. Gladfelter, "Titanium Dioxide (TiO_2)-Based Gate Insulators," *IBM J. Res. Dev.*, **43** [3] 383–92 (1999).

[9]J.-H. Kim, S. Lee, and H.-S. Im, "The Effect of Target Density and its Morphology on TiO_2 Thin Films Grown on Si(100) by PLD," *Appl. Surf. Sci.*, **151** [1–2] 6–16 (1999).

[10]H. Tang, K. Prasad, R. Sanjines, P. Schmid, and F. Levy, "Electrical and Optical Properties of TiO_2 Anatase Thin Films," *J. Appl. Phys.*, **75** [4] 2042–7 (1994).

[11]J. Akedo, "Aerosol Deposition of Ceramic Thick Films at Room Temperature: Densification Mechanism of Ceramic Layers," *J. Am. Ceram. Soc.*, **89** [6] 1834–9 (2006).

[12]J. Akedo, "Room Temperature Impact Consolidation (RTIC) of Fine Ceramic Powder by Aerosol Deposition Method and Applications to Microdevices," *J. Therm. Spray Technol.*, **17** [2] 181–98 (2008).

[13]S. Q. Fan, C. J. Li, C. X. Li, G. J. Liu, G. J. Yang, and L. Z. Zhang, "Preliminary Study of Performance of Dye-Sensitized Solar Cell of Nano-TiO_2 Coating Deposited by Vacuum Cold Spraying," *Mater. Trans.*, **47** [7] 1703–9 (2006).

[14]S. Q. Fan, C. J. Li, G. J. Yang, L. Z. Zhang, J. C. Gao, and Y. X. Xi, "Fabrication of Nano-TiO_2 Coating for Dye-Sensitized Solar Cell by Vacuum Cold Spraying at Room Temperature," *J. Therm. Spray Technol.*, **16** [5] 893–7 (2007).

[15]J. Ryu, D. S. Park, B. D. Hahn, J. J. Choi, W. H. Yoon, K. Y. Kim, and H. S. Yun, "Photocatalytic TiO_2 Thin Films by Aerosol-Deposition: From Micron-Sized Particles to Nano-Grained Thin Film at Room Temperature," *Appl. Catal. B Environ.*, **83** [1–2] 1–7 (2008).

[16]J. J. Park, M. W. Lee, S. S. Yoon, H. Y. Kim, S. C. James, S. D. Heister, S. Chandra, W. H. Yoon, D. S. Park, and J. Ryu, "Supersonic Nozzle Flow Simulations for Particle Coating Applications: Effects of Shockwaves, Nozzle Geometry, Ambient Pressure, and Substrate Location upon Flow Characteristics," *J. Therm. Spray Technol.*, **20**, 514–22 (2011).

[17]M. Lebedev, J. Akedo, K. Mori, and T. Eiju, "Simple Self-Selective Method of Velocity Measurement for Particles in Impact-Based Deposition," *J. Vac. Sci. Technol. A Vac. Sur. Films*, **18**, 563–6 (2000).

[18]H. Katanoda and K. Matsuo, "Gasdynamic Simulation of Aerosol Deposition Method," *Mater. Trans.*, **47** [7] 1620–5 (2006).

[19]M. Lee, J. Park, D. Kim, S. Yoon, H. Kim, D. Kim, S. James, S. Chandra, T. Coyle, and J. Ryu, "Optimization of Supersonic Nozzle Flow for Titanium Dioxide Thin-film Coating by Aerosol Deposition," *J. Aerosol Sci.*, **42** [11] 771–80 (2011).

[20]F. J. Humphreys and M. Hatherly, *Recrystallization and Related Annealing Phenomena*. Elsevier, Amsterdam, 2004.

[21]K. H. Kim, M. Watanabe, J. Kawakita, and S. Kuroda, "Grain Refinement in a Single Titanium Powder Particle Impacted at High Velocity," *Scripta Mater.*, **59**, 768–71 (2008).

[22]J. Yu, X. Zhao, Q. Zhao, and G. Wang, "Preparation and Characterization of Super-Hydrophilic Porous TiO_2 Coating Films," *Mater. Chem. Phys.*, **68** [1–3] 253–9 (2001).

[23]M. Faustini, L. Nicole, C. Boissiere, P. Innocenzi, C. Sanchez, and D. Grosso, "Hydrophobic, Antireflective, Self-Cleaning, and Antifogging Sol– Gel Coatings: An Example of Multifunctional Nanostructured Materials for Photovoltaic Cells," *Chem. Mater.*, **22**, 4406–13 (2010).

[24]G. K. Mor, O. K. Varghese, M. Paulose, K. Shankar, and C. A. Grimes, "A Review on Highly Ordered, Vertically Oriented TiO_2 Nanotube Arrays: Fabrication, Material Properties, and Solar Energy Applications," *Solar Energy Mater. Sol. Cells*, **90** [14] 2011–75 (2006).

[25]J. Shui, Y. Yu, and C. Chen, "Deposition Conditions in Tailoring the Morphology of Highly Porous Reticular Films Prepared by Electrostatic Spray Deposition (ESD) Technique," *Appl. Surf. Sci.*, **253** [5] 2379–85 (2006).

[26]Z. Liu, X. Zhang, S. Nishimoto, M. Jin, D. A. Tryk, T. Murakami, and A. Fujishima, "Highly Ordered TiO_2 Nanotube Arrays with Controllable Length for Photoelectrocatalytic Degradation of Phenol," *J. Phys. Chem. C*, **112** [1] 253–9 (2008).

[27]H. Yang, A. Kuperman, N. Coombs, S. Mamiche-Afara, and G. A. Ozin, "Synthesis of Oriented Films of Mesoporous Silica on Mica," *Nature*, **379** [6567] 703–5 (1996).

[28]R. Uhlhorn, K. Keizer, and A. Burggraaf, "Gas Transport and Separation with Ceramic Membranes. Part II. Synthesis and Separation Properties of Microporous Membranes," *J. Membr. Sci.*, **66** [2–3] 271–87 (1992).

[29]J. Ritchie, J. Richardson, and D. Luss, "Ceramic Membrane Reactor for Synthesis Gas Production," *AIChE J.*, **47** [9] 2092–101 (2001).

[30]J. Lin and C. W. Brown, "Sol-Gel Glass as a Matrix for Chemical and Biochemical Sensing," *TrAC, Trends Anal. Chem.*, **16** [4] 200–11 (1997).

[31]C. Chen, E. Kelder, and J. Schoonman, "Effect of Layer Morphology on the Lithium-Ion Diffusion in Thin Li_xCoO_2 Films," *J. Mater. Sci. Lett.*, **16** [24] 1967–9 (1997).

[32]J. Shui, G. Jiang, S. Xie, and C. Chen, "Thin Films of Lithium Manganese Oxide Spinel as Cathode Materials for Secondary Lithium Batteries," *Electrochim. Acta*, **49** [13] 2209–13 (2004).

[33]J. M. Wu and H. X. Xue, "Photocatalytic Active Titania Nanowire Arrays on Ti Substrates," *J. Am. Ceram. Soc.*, **92** [9] 2139–43 (2009).

[34]F. Iskandar, A. B. D. Nandiyanto, K. M. Yun, C. J. Hogan Jr, K. Okuyama, and P. Biswas, "Enhanced Photocatalytic Performance of Brookite TiO_2 Macroporous Particles Prepared by Spray Drying with Colloidal Templating," *Adv. Mater.*, **19** [10] 1408–12 (2007).

[35]M. Koelsch, S. Cassaignon, J. Guillemoles, and J. Jolivet, "Comparison of Optical and Electrochemical Properties of Anatase and Brookite TiO_2 Synthesized by the Sol–Gel Method," *Thin Solid Films*, **403**, 312–9 (2002).

[36]T. Shibata, H. Irie, M. Ohmori, A. Nakajima, T. Watanabe, and K. Hashimoto, "Comparison of Photochemical Properties of Brookite and Anatase TiO_2 Films," *PCCP*, **6** [6] 1359–62 (2004).

[37]M. Lebedev, J. Akedo, A. Iwata, S. Sugimoto, and K. Inomata, "NiZnCu Ferrite Thick Film with Nano Scale Crystallites Formed by the Aerosol Deposition Method," *J. Am. Ceram. Soc.*, **87** [9] 1621–4 (2004).

[38]M. Miwa, A. Nakajima, A. Fujishima, K. Hashimoto, and T. Watanabe, "Effects of the Surface Roughness on Sliding Angles of Water Droplets on Superhydrophobic Surfaces," *Langmuir*, **16** [13] 5754–60 (2000).

[39]T. Watanabe, S. Fukayama, M. Miyauchi, A. Fujishima, and K. Hashimoto, "Photocatalytic Activity and Photo-Induced Wettability Conversion of TiO_2 Thin Film Prepared by Sol-Gel Process on a Soda-Lime Glass," *J. Sol-Gel. Sci. Technol.*, **19** [1] 71–6 (2000).

[40]R. Fretwell and P. Douglas, "An Active, Robust and Transparent Nanocrystalline Anatase TiO_2 Thin Film — Preparation, Characterisation and the Kinetics of Photodegradation of Model Pollutants," *J. Photochem. Photobiol. A Chem.*, **143** [2–3] 229–40 (2001).

[41]X. Zhang, M. Jin, Z. Liu, D. A. Tryk, S. Nishimoto, T. Murakami, and A. Fujishima, "Superhydrophobic TiO_2 Surfaces: Preparation, Photocatalytic Wettability Conversion, and Superhydrophobic-Superhydrophilic Patterning," *J. Phys. Chem. C*, **111** [39] 14521–9 (2007). □